Gondwana Research 85 (2020) 76–83

Contents lists available at ScienceDirect

Gondwana Research

journal homepage: www.elsevier.com/locate/gr

GR letter

Carbonatite and highly peralkaline nephelinite melts from Oldoinyo Lengai Volcano, Tanzania: The role of natrite-normative fluid degassing

Márta Berkesi [a], Enikő Bali [b], Robert J. Bodnar [c], Ábel Szabó [a], Tibor Guzmics [a,*]

[a] Lithosphere Fluid Research Lab, Eötvös University Budapest, 1117 Budapest, Pázmány P. stny 1/C, Hungary
[b] Nordic Volcanological Center, Institute of Earth Sciences, University of Iceland, Askja Building, Sturlugata 7, 101 Reykjavík, Iceland
[c] Fluids Research Group, Virginia Polytechnic Institute and State University, 4053A Derring Hall, Blacksburg, VA 24061, USA

ARTICLE INFO

Article history:
Received 20 December 2019
Received in revised form 5 March 2020
Accepted 25 March 2020
Available online 22 May 2020

Handling Editor: T. Tsunogae

ABSTRACT

Oldoinyo Lengai, located in the Gregory Rift in Tanzania, is a world-famous volcano owing to its uniqueness in producing natrocarbonatite melts and because of its extremely high CO_2 flux. The volcano is constructed of highly peralkaline [PI = molar $(Na_2O + K_2O)/Al_2O_3 > 2–3$] nephelinite and phonolites, both of which likely coexisted with carbonate melt and a CO_2-rich fluid before eruption. Results of a detailed melt inclusion study of the Oldoinyo Lengai nephelinite provide insights into the important role of degassing of CO_2-rich vapor in the formation of natrocarbonatite and highly peralkaline nephelinites. Nepheline phenocrysts trapped primary melt inclusions at 750–800 °C, representing an evolved state of the magmas beneath Oldoinyo Lengai. Raman spectroscopy, heating-quenching experiments, low current EDS and EPMA analyses of quenched melt inclusions suggest that at this temperature, a dominantly natrite$_{ss}$-normative, F-rich (7–14 wt%) carbonate melt and an extremely peralkaline (PI = 3.2–7.9), iron-rich nephelinite melt coexisted following degassing of a $CO_2 + H_2O$-vapor. We furthermore hypothesize that the degassing led to re-equilibration between the melt and liquid phases that remained and involved 1/ mixing between the residual (after degassing) alkali carbonate liquid and an F-rich carbonate melt and 2/ enrichment of the coexisting nephelinite melt in alkalis. We suggest that in the geological past similar processes were responsible for generating highly peralkaline silicate melts in continental rift tectonic settings worldwide.

1. Introduction

Oldoinyo Lengai, located in Gregory Rift (East African Rift System) in Tanzania, is one of the best-known volcanoes in the world, and is the only active volcano that periodically produces peralkaline nephelinite and phonolite lavas together with small amounts of natrocarbonatite melts (Donaldson et al., 1987; Dawson, 1998). Fresh natrocarbonatite rock dominantly consists of natrite$_{ss}$ [natrite solid solution = gregoryite $(Na_2,K_2,Ca)CO_3$] and nyerereite$_{ss}$ [nyerereite-fairchildite solid solution, $(Na,K)_2Ca(CO_3)_2$] phenocrysts together with fluorite- (CaF_2) bearing groundmass (Keller and Krafft, 1990; Peterson, 1990). Mixed natrocarbonatite-silicate ashes produced during the 1966–67 and 2007–2008 eruptions (Dawson et al., 1992; Mitchell and Dawson, 2007; Mattson and Reusser, 2010) and peralkaline nephelinite globules found in natrocarbonatite ashes from the 1993 eruption (Church and Jones, 1995) indicate immiscibility between a natrocarbonatite and a peralkaline nephelinite melt before eruption. Additionally, evidence of silicate-carbonate immiscibility is clearly present in melt inclusions from Oldoinyo Lengai (Mitchell, 2009; Mitchell and Dawson, 2012; Sharygin et al., 2012) and from the adjacent Kerimasi volcano (Guzmics et al., 2012, 2019).

Oldoinyo Lengai is dominantly composed of pyroclastic rocks (Dawson, 1962), suggesting intense volatile degassing (de Moor et al., 2013) during eruption. During the explosive eruptive activity at Oldoinyo Lengai, the CO_2-flux is extremely high (Brantley and Koepenick, 1995), making this volcano one of the most significant CO_2 emitters on Earth. The CO_2 emissions are also accompanied by the release of H_2O, which represents 24–34 mol% of the degassing volatile phase (Koepenick et al., 1996). All of these observations strongly suggest that at the subvolcanic level a CO_2-bearing fluid is associated with immiscible carbonate-silicate melts.

The formation mechanism that generates the Earth's highly peralkaline [molar $(Na_2O + K_2O)/Al_2O_3 > 2$, de Moor et al., 2013; Mitchell, 2009] nephelinites is one of the most controversial topics concerning the genesis of alkaline rocks. Earlier studies suggested a relationship between degassing CO_2 and the formation of highly peralkaline nephelinite melts. These include carbonatite melt injection into a clinopyroxene-rich crystal mush in the subvolcanic environment (Weidendorfer et al., 2019) or dissolution of carbonatite melts into a non-conjugate nephelinite melt (Mitchell and Dawson, 2007; Bosshard-Stadlin et al., 2014). In contrast to these models, Guzmics

* Corresponding author.
E-mail address: tibor.guzmics@gmail.com (T. Guzmics).

https://doi.org/10.1016/j.gr.2020.03.013

et al. (2019) discovered an immiscible alkali carbonate fluid phase coexisting with silicate and carbonate melts (without carbonatite or pyroxene dissolution) at the nearby Kerimasi volcano. Interestingly, the alkali carbonate fluid phase has CO_2/H_2O ratios that are similar to the volcanic emissions at Oldoinyo Lengai (Koepenick et al., 1996). The degassing of $CO_2 + H_2O$ from the fluid produces a liquid residue that is expected to be very rich in $natrite_{ss}$ component.

In this paper, we present a detailed melt inclusion study of the Oldoinyo Lengai nephelinite. We demonstrate the role of degassing in the formation of extremely peralkaline nephelinites. As a similar fluid phase potentially exists in all magmatic systems of this type, our model may be generally applicable to the formation of highly peralkaline, SiO_2-undersaturated lavas occurring worldwide (Marks and Markl, 2017; Platz et al., 2004; Rooney, 2019; Woolley et al., 1995).

2. Methods

The nephelinite rock was studied in five doubly-polished thin sections. Microthermometric data from the melt inclusions were collected using a Linkam TS 1500 heating-cooling stage mounted on a Nikon Eclipse LV100PL petrographic microscope at the Lithosphere Fluid Research Lab, Eötvös University, Budapest. The heating rate was 10 °C/min, with a maximum temperature of 1000 °C. The uncertainty of reported temperatures does not exceed 5 degrees Celsius.

Raman microspectroscopy was conducted at the Faculty of Science Research and Instrument Core Facility of Eötvös University, Budapest (ELTE FS-RICF). We used a confocal HORIBA Labram HR (high resolution) 800 mm spectrometer with Nd:YAG laser ($\lambda = 532$ nm) excitation, a 1800 grooves/mm optical grating, a 50–200 μm confocal hole, 2–50 s acquisition time, and a 100× objective (numerical aperture 0.9). The laser spot size (lateral) was 1.2 μm, and the depth resolution was 1.7 μm (using a 50 μm confocal hole and 100× objective). The laser power was 130 mW at the source and ~50 mW at the sample surface. The spectral resolution was 0.7 cm^{-1} at 1398.5 cm^{-1} (full width at half maximum of one neon line). Data evaluation (background fitting and peak fitting using the Gaussian–Lorentzian sum profiles) was carried out using LabSpec software. Minerals and fluid components were identified based on comparison with the databases of Frezzotti et al. (2012) and RRUFF (rruff.info).

Heating-quenching experiments on melt inclusions followed the same method as described by Guzmics et al. (2012, 2019). We used a Carl-Zeiss Jena high-temperature (1 atm) furnace to reproduce the characteristic melt phases that were present at the time of trapping. Handpicked single nepheline grains (n = 72) were encapsulated in graphite containers to prevent oxidation during the experiments. Temperature during the experiments was 800 °C, with an uncertainty of ± 20 degrees Celsius. The heating rate from room temperature was 15–20 degrees Celsius/min. Quenched melts were produced with a quenching rate of 300–350 °C/s. The quenched melt inclusions were exposed at the surface by polishing using dry corundum powder. After exposure, the grains were placed in oil to prevent alteration of the quenched carbonate melts when in contact with humid air.

In order to obtain the major element composition of the phenocrysts and the quenched melts in the exposed nepheline-hosted melt inclusions, a Quantax75 EDS-SDD in combination with a Hitachi TM4000Plus microscope was used at ELTE FS-RICF with instrument settings of 15 kV accelerating voltage, 200 pA beam current and 15 s counting times. Low current conditions were used to minimize volatilization and thus underestimation of Na in the quenched melt phases. Oil was removed from the grains using a tissue immediately before the analyses (without using water). Replicate analyses of different areas of the melt inclusions show no significant compositional variation within a given inclusion. Control measurements on the nepheline and clinopyroxene grains as well as on the silicate glass in the melt inclusions were obtained by using a JEOL JXA8230 electron microprobe (EPMA) with wavelength-dispersive spectrometry at the Institute of Earth Sciences, University of

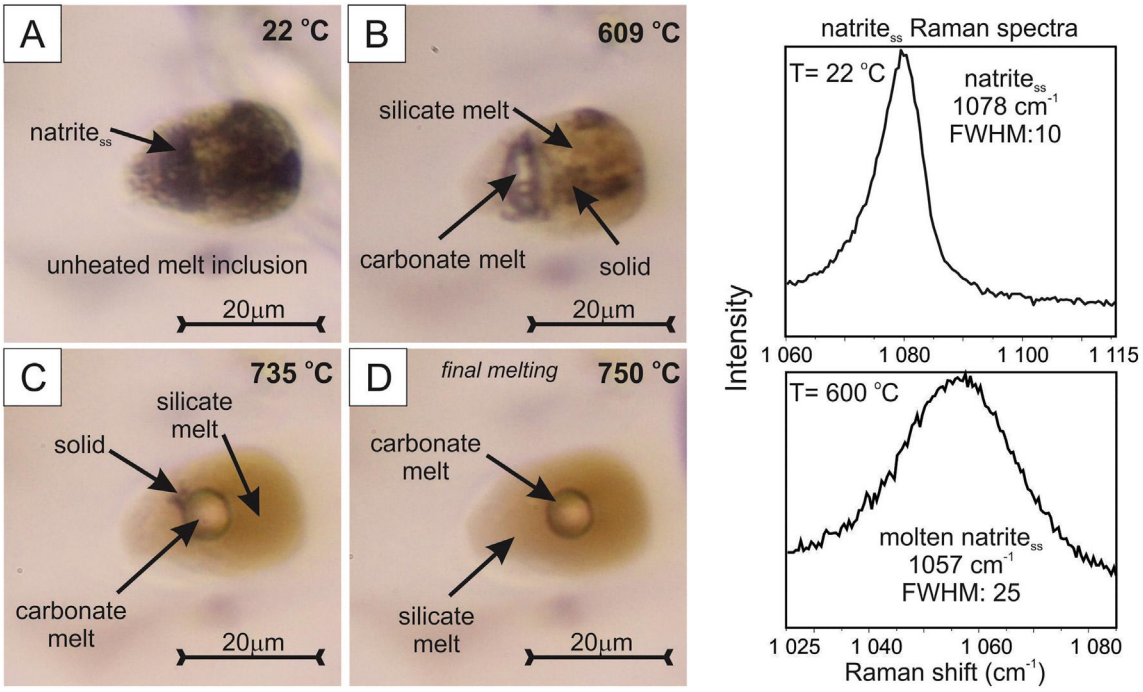

Fig. 1. Representative photomicrographs of a nepheline-hosted melt inclusion during microthermometry (transmitted light, 1 nicol). A: At room temperature (22 °C) the unheated melt inclusion is fully crystallized. The upper Raman spectrum was collected with the laser focused on the carbonate-rich part (darker parts) of the melt inclusion and shows the characteristic band of $natrite_{ss}$ (natrite solid solution). B: Immiscible silicate (brownish) and carbonate (white) melts appear at 609 °C together with solids, the lower Raman spectrum shows the characteristics of molten $natrite_{ss}$ (=carbonate melt) at this temperature. C: Further progressive dissolution of solids upon heating with the presence of silicate and carbonate melts (image taken at 735 °C). D: at 750–800 °C, solids were completely dissolved in the melt phases, therefore, these can be considered as entrapment temperatures. FWHM – Full Width at Half Maximum.

Iceland. For silicate glass analysis the accelerating voltage was set as 15 kV, probe current was 2 nA, and the beam size was between 10 and 7 μm. During analyses of pyroxenes we used a beam current of 20 nA and a point beam. Owing to the high concentrations of halogens in quenched carbonate melt and silicate glass, we corrected the oxide wt% values according to 2(F + Cl) = O. The CO_2 content of the carbonate melts was calculated by difference from 100% totals. Natural and synthetic standards were used for instrument calibration, and ZAF corrections were applied.

3. Sampling and petrography

Oldoinyo Lengai is the youngest volcano of the Younger Extrusive volcanic field in the Gregory Rift Valley, northern Tanzania (Dawson, 2012). Volcanic activity in the Gregory Rift started about 10 My ago (Macdonald et al., 2001) in its northern part and propagated to the SW to the site of recent volcanic activity at Oldoinyo Lengai. Oldoinyo Lengai is the only known active volcano in the world producing nephelinite, phonolite and natrocarbonatite tuffs/lava rocks (Dawson, 1962; Mitchell and Dawson, 2007; Mitchell, 2009).

The studied rock is a nephelinite, which is a common rock type occurring at the Oldoinyo Lengai, Tanzania (Dawson, 1962; Mitchell and Dawson, 2007; Mitchell, 2009; Sharygin et al., 2012). We collected a representative volcanic bomb on the northern slope of the volcano. The rock has a porphyritic texture, with euhedral phenocrysts of nepheline (0.2–2 mm) and subordinate clinopyroxene (100–300 μm) (Supplementary Fig. 1), similar to most nephelinite rocks from Oldoinyo Lengai (Klaudius and Keller, 2006). Clinopyroxene phenocrysts are euhedral and zoned. The euhedral habit of the phenocrysts indicates that they are primary liquidus phases (Morse, 1980). The co-precipitation of these two phases is also shown by the presence of mutual inclusions in clinopyroxene and nepheline, such that nepheline hosts euhedral aegirine-augitic clinopyroxene (Supplementary Fig. 1B). Nepheline additionally hosts inclusions of titanite and schorlomite. The matrix is composed of 20–130 μm sized euhedral aegirine-rich clinopyroxene, wollastonite, sodalite, leucite and analcime crystals. Numerous primary melt inclusions are present, both along crystallographic directions in the cores of nephelines (Supplementary Fig. 1C) and randomly distributed within the core of the crystal. Chemical zoning of host nepheline is restricted to a 50–100 μm wide rim that is free of melt inclusions. Unheated melt inclusions are well crystallized (Fig. 1A), which prohibited identification of various melt phases by optical microscopy. This also limited determination of the melt composition(s) by electron microprobe.

4. Results

Zoned clinopyroxene phenocrysts are generally low in Al_2O_3 (<1.5 wt%) and high in Na_2O (1.2–8.5 wt%, Table S1). Rims are enriched in Na_2O and depleted in MgO, as expected during fractional crystallization. In other words, the core is richer in augite component, whereas the rim is enriched in aegirine component. Rims consist of relatively broad zones (up to 100 μm) that consistently become more sodic and iron-rich moving outward. Frequently, the composition of clinopyroxenes enclosed in nepheline phenocrysts is the same as the composition of the inner portion of the rim of clinopyroxene phenocrysts (Table S1). However, nepheline also entrapped augitic clinopyroxene crystals without aegirine-enriched rims. Rims of nepheline phenocrysts show enrichment of FeO^T (2.0–5.6 wt%) relative to the core composition (1.0–2.9 wt%, Table S2), which corresponds to the general trend of increasing Fe-content of nepheline during evolution of paralkaline lavas (Mann et al., 2006).

4.1. Melt inclusions

Room temperature Raman analysis of the carbonate-rich part of unheated nepheline-hosted melt inclusions (n = 45) identified natrite$_{ss}$, with the main band at 1078 cm^{-1} (Thomas et al., 2011) (Fig. 1). Microthermometry of nepheline-hosted melt inclusions (n = 10) combined with Raman analysis showed carbonate melting at 600–610 °C (Fig. 1B) by 1/ the appearance of a meniscus and 2/ significant and sudden broadening of the main Raman band of natrite$_{ss}$ (Full Width at Half

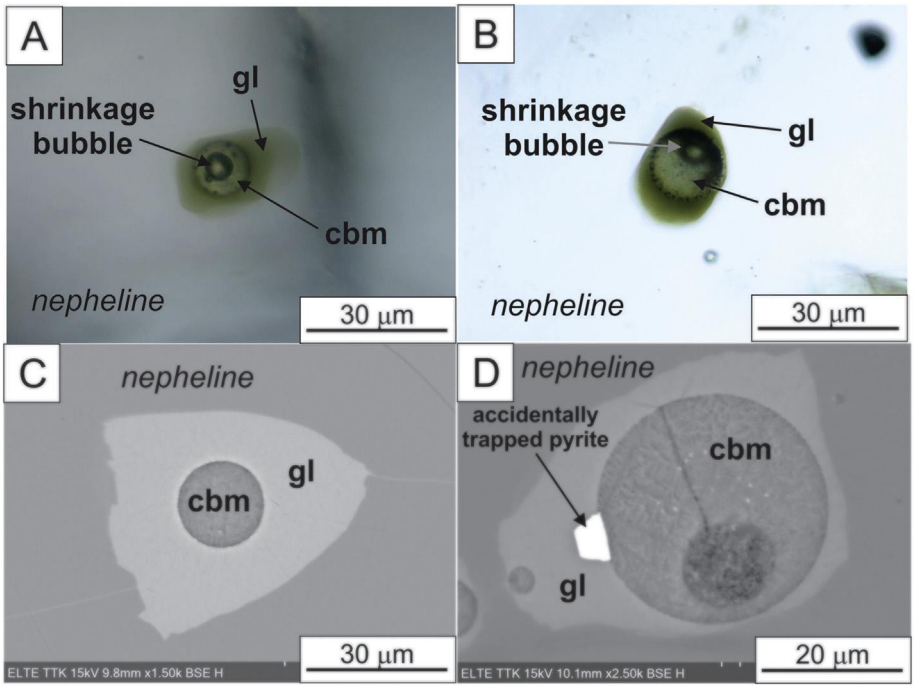

Fig. 2. Representative photomicrographs of nepheline-hosted melt inclusions after heating to 800 °C in the furnace and quenching. A–B: Photomicrographs showing unexposed melt inclusions containing silicate melt quenched as glass (gl), quenched carbonate melt (cbm) and a shrinkage bubble. Transmitted light, 1 nicol. C–D: Back-scattered electron (BSE) images of melt inclusions showing both silicate glass (gl) and quenched carbonate melt (cbm) exposed at the surface. D: The pyrite is an accidentally entrapped (not daughter) mineral.

Maximum increased from ~10 to ~25, Fig. 1). Band broadening is a known Raman spectroscopic response of melting as shown by Rossano and Mysen (2012). At this temperature, a small amount of silicate melt phase was also present (carbonate melt/silicate melt ~60/40 vol%), in addition to a significant volume fraction of solids (Fig. 1B). Further heating resulted in the continuous dissolution of solids into the silicate melt, together with the formation of a clear meniscus between the immiscible silicate and carbonate melts (Fig. 1C). It should be noted that a fluid bubble was not detected above 630 °C during heating experiments. The last solid phase dissolved into the silicate melt between 750 and 800 °C, leaving only a silicate melt and carbonate melt in the inclusion (Fig. 1D). No other phase changes were observed during continued heating (up to 1000 °C). The 750–800 °C temperature range is therefore interpreted to represent the entrapment temperature at the evolved state of the nephelinite-carbonatite system. During cooling of the melt inclusions, a shrinkage bubble (with no detectable CO_2 and H_2O) or, infrequently, a bubble filled with low-density CO_2 appeared at around 550 °C, confirmed by subsequent Raman spectroscopy.

During furnace experiments to form homogeneous melt phases, the furnace temperature was based on the maximum temperature at which all solid daughter phases had dissolved (800 °C) during the microscope heating stage experiments. The melt inclusions were rapidly quenched from 800 °C, and the quenched melt inclusions showed a wide range in the volume ratios of carbonate and silicate melt phases (Fig. 2). The overwhelming majority of the bubbles were interpreted to be shrinkage bubbles owing to the lack of detectable volatiles (CO_2 and H_2O) at room temperature. Silicate glass contained no detectable H_2O (<0.1 wt%) based on room temperature Raman analysis.

Tables 1 and S3–S5 show results of SEM-EDS and EPMA analyses (n = 58) of the quenched and exposed melt inclusions. The silicate melt has a strongly peralkaline [peralkalinity index (PI) = 3.2–7.9], iron- (7.1–12.2 wt%) and alkali-rich ($Na_2O + K_2O$ = 18.6–31.3 wt%) nephelinite composition with 40.4–48.4 wt% SiO_2. The silicate glass composition is also characterized by a significant halogen content, including F (0.8–3.6 wt%) and Cl (0.2–1.4 wt%), in addition to SO_3 (0.2–2.5 wt%).

Table 1
Compositions (wt%) of the immiscible silicate and carbonate melts (quenched after heating to 800 °C) in nepheline-hosted melt inclusions from Oldoinyo Lengai nephelinite, Tanzania.

	Silicate melt n = 30		Carbonate melt n = 26	
	Minimum	Maximum	Minimum	Maximum
SiO_2	40.41	48.42	0.62	1.27
TiO_2	0.78	1.99	bd	0.20
Al_2O_3	5.00	9.29	0.14	0.43
FeO^T	7.19	12.19	0.16	1.26
MnO	0.23	0.74	bd	0.25
MgO	0.47	2.47	0.20	1.85
SrO	bd	0.84	0.34	2.69
CaO	3.13	8.49	15.07	27.64
BaO	0.07	1.03	0.58	1.79
Na_2O	13.45	22.91	19.72	35.34
K_2O	5.12	8.41	3.08	7.26
P_2O_5	0.13	0.87	1.46	4.98
F	0.76	3.56	7.09	13.90
SO_3	0.23	2.53	0.11	6.47
Cl	0.22	1.36	0.79	3.83
Total	98.57	99.50	73.72	83.19
CO_2^*			16.81	26.28
Peralkalinity	3.2	7.9		

FeO^T - all Fe expressed as FeO; oxide values are corrected according to 2F=O and 2Cl=O, peralkalinity - molar $(Na_2O + K_2O)/Al_2O_3$, CO_2^* - CO_2 as carbonate represents difference to 100, bd - below the detection limit. All data presented are from EDS analyses. Individual melt compositions can be found as electronic supplement.

Quenched carbonate melt phases showed total alkalis (expressed in $Na_2O + K_2O$) ranging from 22.8 to 42.6, sometimes exceeding that of fresh natrocarbonatite (total alkalis ~40 wt%, Gittins and Jago, 1998). However, our quenched carbonate melts had slightly higher Ca (expressed in CaO = 15.1–27.7 wt%), P_2O_5 (1.5–5.0 wt%) and much higher F (7.1–13.9 wt%), compared to fresh natrocarbonatite. $CaCO_3/(CaCO_3 + Na_2CO_3 + K_2CO_3)$ ratios of the quenched carbonate melts vary continuously between 0 and 42 (Fig. 3).

5. Discussion

5.1. Origin of the carbonate melts

Fig. 3 shows that the quenched carbonate melts are mainly $natrite_{ss}$-normative i.e. they plot dominantly on the left side of the $natrite_{ss}$–$nyerereite_{ss}$ eutectic. This is in good agreement with our identification of $natrite_{ss}$ during Raman analyses of unheated melt inclusions (Fig. 1). Moreover, the $CaCO_3/(CaCO_3 + Na_2CO_3 + K_2CO_3)$ ratios in quenched carbonate melts vary widely and span the $nyerereite_{ss}$–$natrite_{ss}$ eutectic. In contrast, experimentally produced (Kjarsgaard et al., 1995; Weidendorfer et al., 2017 and references therein) and natural (Nielsen and Veksler, 2002; Guzmics et al., 2012) carbonate melts show calcite- or $nyerereite_{ss}$-normative compositions and plot on the

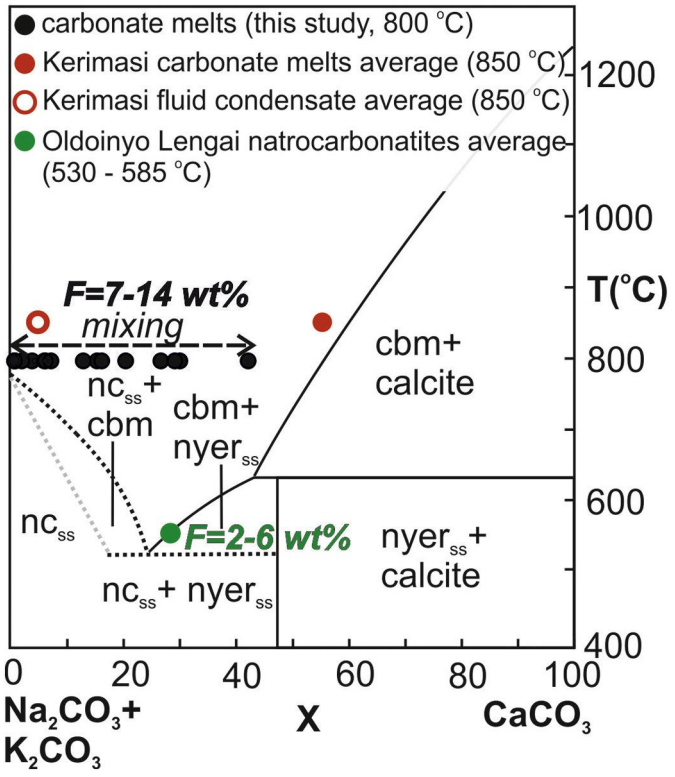

Fig. 3. $(Na_2CO_3 + K_2CO_3)$-$CaCO_3$ (X) versus temperature pseudobinary, modified after Cooper et al. (1975) and Weidendorfer et al. (2017). The gray dotted line represents an estimate for the $natrite_{ss}$ solidus. Black solid and dotted lines indicate the field boundaries at 0.1 GPa. Filled black circles indicate the compositions of individual carbonate melts, quenched from 800 °C. The studied carbonate melts contain 7–14 wt % F, corresponding to 14.4–30.9 wt% CaF_2 component. Dashed arrow shows the compositional range of the mixed carbonate melts. The filled green circle shows the bulk composition of Oldoinyo Lengai natrocarbonatite (Gittins and Jago, 1998), which has a fluorine content of 2–6 wt%. Filled and open red circles indicate the average composition of the carbonate melt (filled) and the fluid condensate (open) from the nearby Kerimasi volcano (nepheline-hosted melt inclusions, Guzmics et al., 2019). cbm – carbonate melt; nc_{ss} – $natrite_{ss}$ = natrite solid solution; $nyer_{ss}$ – nyerereite-fairchildite solid solution; X – mass fraction of the $CaCO_3$ component along the pseudobinary normalized to 100.

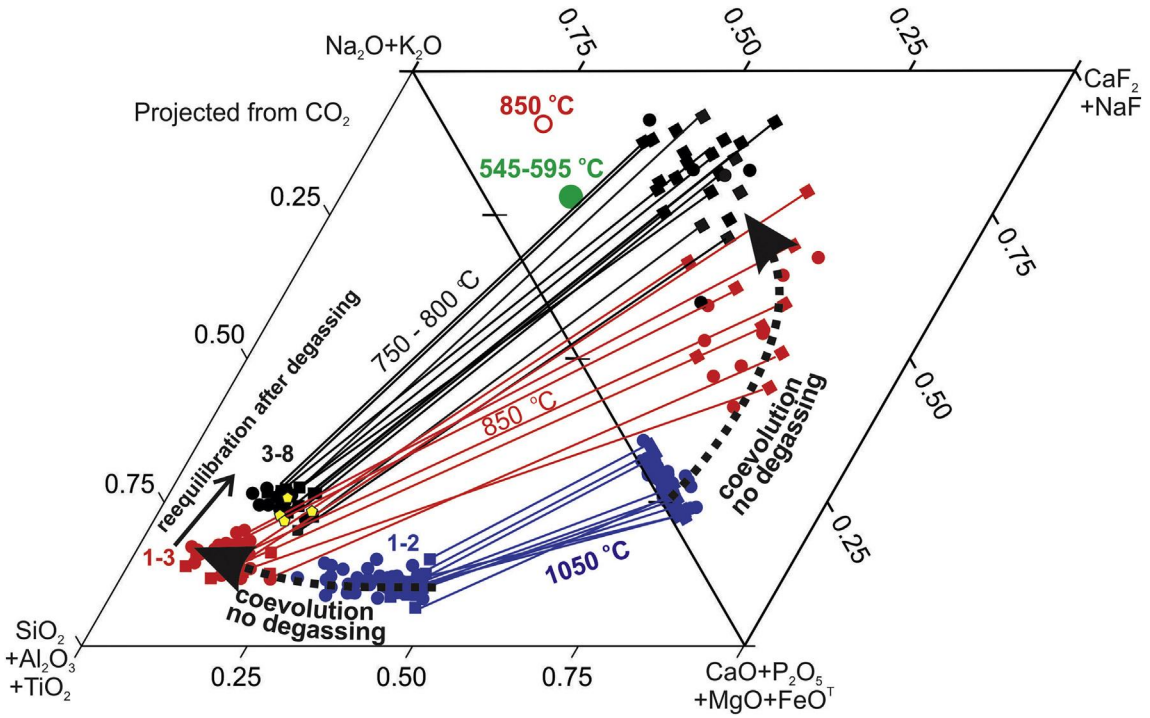

Fig. 4. Modified Hamilton projection (Hamilton et al., 1979) of the quenched silicate and carbonate melts in the studied nepheline-hosted melt inclusions (wt%). Considering the significant normative CaF_2 content in the carbonate melts, a second pseudoternary with NaF + CaF_2 at one corner has been added to the Hamilton projection. Silicate melt compositions are plotted on the left, and carbonate melts are plotted on the right triangle. Black symbols show the melt compositions in this study. For comparison, compositions of natural immiscible carbonate and silicate melt inclusions from the nearby Kerimasi volcano (blue symbols: Guzmics et al., 2012; red symbols: Guzmics et al., 2019) and Oldoinyo Lengai volcano (yellow circles: Mitchell, 2009), are plotted. Tie-lines connect the conjugate silicate–carbonate compositions at the corresponding temperatures (shown in °C on the tie-lines). Numbers with the same color as the silicate melt compositions indicate the range of peralkalinity index [molar $(Na_2O + K_2O)/Al_2O_3$]. The open red circle shows the average composition of fluid condensate from Kerimasi melt inclusions at 850 °C (Guzmics et al., 2019), whereas the green circle plots the average natrocarbonatite composition erupted at 545–595 °C (Gittins and Jago, 1998). Dashed arrows indicate the schematic evolution path of immiscible silicate and carbonate melts coexisting with a fluid phase (no degassing). Black arrow illustrates the compositional change resulting from re-equilibration between the silicate melt and the degassed fluid (residual alkali carbonate liquid). See text for further details.

right side of the nyerereite$_{ss}$–natrite$_{ss}$ eutectic (Fig. 3). Based on phase equilibrium constraints, a carbonate melt having a nyerereite$_{ss}$-normative composition cannot propagate through and beyond the eutectic point to become natrite$_{ss}$-normative. In contrast, an alkali carbonate fluid phase (which is immiscible with an F-rich calcite- or nyerereite$_{ss}$-normative carbonate melt and a slightly peralkaline nephelinite melt at 850 °C) can be natrite$_{ss}$-normative (Guzmics et al., 2019). It is likely, therefore, that natrite$_{ss}$-normative carbonate melts observed at Oldoinyo Lengai originated from such a fluid-phase. Moreover, fenitizing fluids are also alkaline, mainly consisting of Na and C, and the source of these fluids is the carbonatite melts (Cooper et al., 2016).

Studied carbonate melts contain significant concentrations of Ca (expressed in CaO = 15.1–27.6 wt%); in addition, they are extremely rich in F (7.1–13.9 wt%, Tables 1, S4 and S5). Fluorine is thought to be a key component in the formation of alkaline carbonate melts, as 1) it suppresses the calcite liquidus in Ca-Na carbonate melts and therefore restricts crystallization (Jago and Gittins, 1991) and 2) contributes to breaking of the "thermal barrier" on nyerereite$_{ss}$ compositions (Weidendorfer et al., 2017) observed in the Na_2CO_3-K_2CO_3-$CaCO_3$ system (Cooper et al., 1975). Experiments by Williams and Knittle (2003) suggest that fluorine disrupts the carbonate units in the melt and may form Ca-F bonds. This can be an important process in the formation of Oldoinyo Lengai natrocarbonatites (which have 2–6 wt% bulk fluorine contents, Keller and Krafft, 1990) as they contain fluorite (CaF_2) (Mitchell and Dawson, 2007; Kervyn et al., 2008). The dominance of Ca-F bonds (e.g., the presence of dissolved CaF_2) in the studied inclusion-hosted carbonatite melts is suggested by their natrite$_{ss}$-normative nature and by the high normative CaF_2-contents (14.4–30.9 wt%). This indicates that essentially all F in the carbonate melts is associated with Ca. It should be noted, however, that addition of CaF_2 to nyerereite$_{ss}$-normative carbonate melts will not result in natrite$_{ss}$-normative melt compositions. This further highlights the significance of the alkali carbonate fluid phase during formation of natrite$_{ss}$-normative melt compositions. Results of this study additionally emphasize that carbonate melt evolution cannot be fully understood if their composition is interpreted based on the widely used Hamilton projection (Freestone and Hamilton, 1980), as in this case fluorine is not considered.

5.2. Effect of degassing and sources of CO_2-dominated vapor phase

Phase separation in an alkali carbonate fluid produces a $CO_2 + H_2O$-rich vapor and a natrite$_{ss}$-normative liquid phase. When the $CO_2 + H_2O$-rich phase degasses, a residual alkali carbonate liquid remains (Guzmics et al., 2019). Failure to detect any evidence of CO_2 or H_2O in either the bubble phase of the quenched melt inclusions or in the silicate glasses supports an almost complete outgassing of $CO_2 + H_2O$ before entrapment of melt inclusions. CO_2-rich, H_2O-bearing degassing is a common process during the volcanic history of Oldoinyo Lengai (Brantley and Koepenick, 1995; Pyle et al., 1995; Koepenick et al., 1996; Nielsen and Veksler, 2002) and is thought to play an important role in 1) inducing crystallization in response to decompression degassing (de Moor et al., 2013) and 2) prevents the exsolution of natrocarbonatite from peralkaline nephelinite melt (Dawson, 1998). Our results indicate, however, that degassing (i.e. loss of $CO_2 + H_2O$ vapor) drives the immiscible carbonate melt and the degassed, residual

natrite$_{ss}$-normative liquid to form a mixed alkali-rich carbonate melt phase (Fig. 3), which is immiscible with the peralkaline nephelinite melt (Fig. 2). This mixing (Fig. 3) is likely responsible for producing the Oldoinyo Lengai natrocarbonatite compositions, with CaF_2 fractionation taking place between ~750–800 °C and ~ 550 °C (e.g. the eruption temperature of natrocarbonatite, Keller and Krafft, 1990) (Fig. 4). Thus, our model suggests that the majority of CO_2 is liberated from the alkali carbonate fluid phase. However, some CO_2 was generated during re-equilibration (see details in the next chapter) between the residual alkali carbonate liquid and the silicate melt, according to the following example:

$2(Na,K)_2CO_3$ component in residual alkali carbonate liquid
$+ (Na,K)AlSi_3O_8$ component in silicate melt→$(Na,K)AlSiO_4$
$+ 2(Na,K)_2SiO_3$ components in silicate melt $+ 2CO_2$ vapor↑

5.3. Highly peralkaline nephelinite melt formation

The studied carbonate melts coexist with highly peralkaline (PI = 3.2–7.9) nephelinite melts (Fig. 4, Tables 1 and S3) having high normative $Na_2SiO_3 + K_2SiO_3$ contents (19.3–44.7 wt%). During crystal fractionation of aluminous clinopyroxene at high temperatures (≥900 °C), a maximum PI value of 1.2–1.5 is possible in nephelinite-phonolite melts (Peterson, 1989; Weidendorfer et al., 2019). During further silicate melt evolution, the melt peralkalinity remains almost constant or decreases once the co-crystallization of nepheline and sodic clinopyroxene commences (Supplementary Fig. 1). Other constituent minerals of peralkaline igneous rocks are Na-rich and Al-poor (Marks and Markl, 2017), thus the crystal-fractionation-controlled increase of peralkalinity in silicate melts is limited by the formation of Al-rich clinopyroxene (Peterson, 1989), which cannot explain the high PI values observed in the studied nephelinite melts at Oldoinyo Lengai.

Recent models propose more complex processes for the formation of strongly peralkaline nephelinite melts at Oldoinyo Lengai via augitic clinopyroxene dissolution by a Ca-rich carbonate melt, which triggers formation of peralkaline silicate melt with unusually low (≤1.5 wt%) Al_2O_3 and normative nepheline-content, peritectic melilite and/or ghost-shaped clinopyroxene crystals at temperatures of 925–1000 °C (Weidendorfer et al., 2019). Our results do not support this model because 1) mutual euhedral crystal inclusions of aegirin-augite and nepheline (Supplementary Fig. 1), together with entrapped primary melt inclusions in nepheline, suggest that at the time of melt entrapment nepheline and aegirine-augitic clinopyroxene were co-crystallizing, 2) the entrapment temperature (750–800 °C) of our melt inclusions is lower than the experimentally determined temperature for clinopyroxene dissolution (Weidendorfer et al., 2019), 3) the studied rocks do not contain remnants or products of an earlier carbonate-melt induced dissolution reaction, such as peritectic melilite or ghost-shaped augitic cores of clinopyroxenes and 4) the elevated Al_2O_3 contents (5.0–9.3 wt%, Table S3) of studied melt inclusion-hosted nephelinite melts is unlikely to be derived from a silicate melt that has almost no normative nepheline-content (Al_2O_3 ≤ 1.5 wt%) by crystal fractionation of nepheline (the main rock forming mineral in our samples). High peralkalinity in glasses of nephelinite rock from Oldoinyo Lengai was reported by Dawson (1998), who suggested that CO_2 loss by explosive eruptions leads to carbonate undersaturation in silicate melt and, thus, precludes the unmixing of carbonatite melt from nephelinite melt. This scenario can be excluded for the studied nephelinite owing to the large variations in volumetric proportions of immiscible carbonate and silicate melts in different melt inclusions (Fig. 2). These variations clearly indicate that these phases were immiscible 1/ at the time of entrapment and 2/ after outgassing of the alkali carbonate fluid (e.g. loss of vapor $CO_2 + H_2O$), based on the lack of detectable CO_2 and H_2O in the bubble and the silicate glass of the quenched melt inclusions. The composition of extremely peralkaline nephelinitic glass in immiscible silicate-carbonate melt inclusions hosted in nepheline phenocrysts from combeite ($Na_2Ca_2Si_3O_9$) nephelinite rock at Nasira scoria cone (north side of Oldoinyo Lengai) was interpreted to be the result of assimilation of natrocarbonatite melt into a nephelinite melt (Mitchell and Dawson, 2012). Such assimilation is driven by the concept of a hotter nephelinite melt being injected into a pre-existing, separately evolved natrocarbonatitic melt or rock in one of the sub-chambers beneath the Oldoinyo Lengai plumbing system (Dawson et al., 1992; Mattson and Reusser, 2010). However, extremely high F concentrations (7.1–13.9 wt%) in the studied carbonate melts cannot be explained from an independently evolving carbonate melt (Guzmics et al., 2019); instead, it indicates the coevolution of carbonatite with a nephelinite-phonolite melt from higher temperatures.

The majority of previous studies do not report the compositions of the coexisting immiscible fluid phase, despite the fact that fluid is a common phase during evolution of almost all igneous systems. Moreover, recent results of Guzmics et al. (2019) showed that the immiscible fluid phase is extremely enriched in $Na_2O + K_2O$ and, therefore, has significant potential to increase peralkalinity in the coexisting silicate melt during re-equilibration. Based on results presented above, we suggest that extreme peralkalinity of the nephelinite melt is the result of re-equilibration (Eq. 1) between the outgassed, residual alkali carbonate liquid and the silicate melt. If we consider the evolution of an immiscible carbonate-nephelinite-fluid system from high temperatures, the following scenario (Fig. 5) is plausible in the plumbing system. At ~1100 °C, a carbonated nephelinite melt that formed by partial melting of a carbonate-bearing mantle is present. At ~1050 °C and crustal pressures (0.5–1 GPa), the composition of the melt evolves due to fractional crystallization of augitic clinopyroxene and nepheline, and results in immiscibility between an MgO- and alkali-bearing, CaO- and FeO-rich nepheline melt and an F-bearing (up to 1.91 wt%, Guzmics et al., 2012), CaO- and P_2O_5-rich carbonate melt ± fluid phase ± sulfide melt (Figs. 4 and 5A.). In this case, nephelinite melt is considered to be the volumetrically dominant melt phase (Fig. 5A). Its peralkalinity ranges between 1 and 2. Progressive coevolution of the immiscible carbonate and nephelinite melt from ~1050 °C to 850 °C contributes to formation of an extremely F-rich (5–14 wt%) nyerereite$_{ss}$-normative carbonate melt, and the peralkalinity of the coexisting nephelinite-phonolite melt can reach 1–3 (Figs. 4 and 5B). At this stage, a natrite$_{ss}$-normative alkali carbonate fluid is immiscible with both the carbonate and silicate melts (Guzmics et al., 2019). At ~850 °C, the volume of the carbonate melt as well as the fluid phase, relative to the nephelinite-phonolite melt, becomes significant (fluid phase accumulation, Fig. 5B). Due to a pressure decrease, the fluid phase separates to produce a natrite$_{ss}$-normative alkali carbonate liquid and a $CO_2 + H_2O$-dominated vapor. Outgassing (vapor loss) of the fluid phase at ~750–800 °C induces re-equilibration (including redistribution of alkalis, Eq. (1)) between the remaining liquid and melt phases. This includes a mixing between the F-rich nyerereite$_{ss}$-normative carbonate melt and a natrite$_{ss}$-normative alkali carbonate liquid, together with Na and K enrichment of the coexisting nephelinite melt (Fig. 5C). According to the reaction in Eq. (1), the SiO_2-content of the silicate melt before outgassing was likely higher, even reaching phonolitic compositions (Fig. 4). Nevertheless, this re-equilibration process leads to the formation of highly peralkaline (PI = 3.2–7.9, Table 1) nephelinite melt (Figs. 4 and 5). The significant increase in the peralkalinity can only be explained if we assume that the volume of the nephelinite melt is less than that of the accumulated fluid and carbonate melt (Figs. 5B and C). The volumetric dominance of the immiscible carbonate melt is indicated by microthermometric results that show that at low temperature (600–610 °C) the nephelinite melt was partly crystallized, in contrast to the carbonate melt phase (Fig. 1), and by the ash deposits from the 2008 eruption at Oldoinyo Lengai in which the natrocarbonatite:nephelinite volume ratio was estimated to be 4:1 (Keller et al., 2010; Mattson and Reusser, 2010).

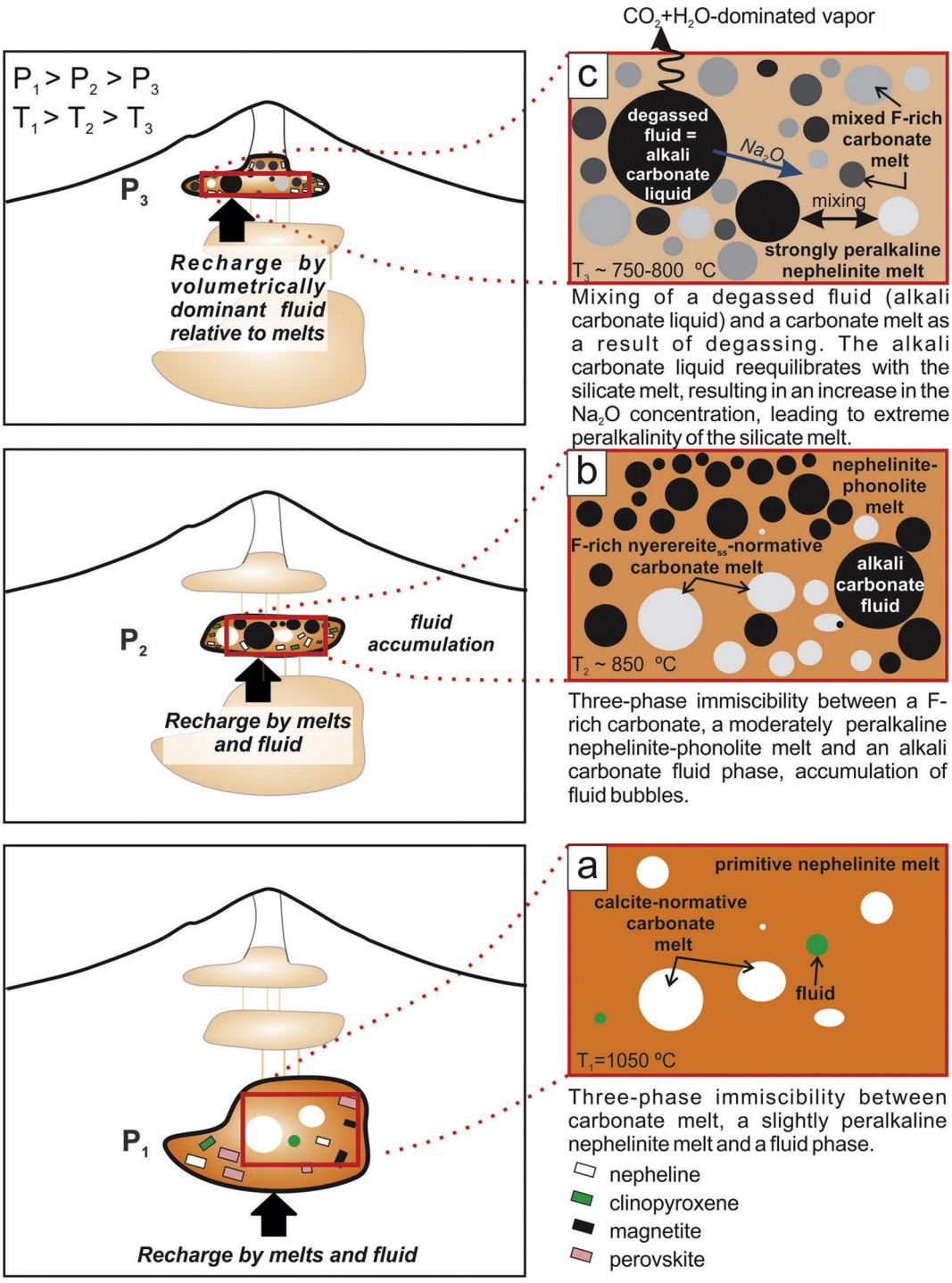

Fig. 5. Schematic model for the evolution of melt and fluid phases from ~1050 °C to 750–800 °C in the open magmatic plumbing system of the Oldoinyo Lengai volcano. Panels a, b, and c are schematic representations of the magma at different stages as the system evolves from higher towards lower temperature ($T_1 > T_2 > T_3$) and pressure ($P_1 > P_2 > P_3$). Schematic position in the magmatic system corresponding to panels a, b and c is illustrated by red squares. The panels a–c focus on the evolution of the melt and fluid phases; the crystallizing minerals are not shown. A description of processes occurring in each stage (a, b, and c) is provided beneath each panel.

6. Concluding remarks

We document the co-entrapment of F-rich (7–14 wt%) and natrite$_{ss}$-normative carbonate melt with an immiscible highly peralkaline (PI = 3.2–7.9) nephelinite melt in nepheline phenocrysts in nephelinite from Oldoinyo Lengai volcano, Tanzania. Melt entrapment temperatures are estimated to be ~750–800 °C. Natrite$_{ss}$-normative carbonate melts likely originated from an alkali carbonate fluid phase after degassing. After the $CO_2 + H_2O$-dominated vapor was lost from the system due to degassing, the remaining phases re-equilibrated. This resulted in: 1) mixing between the residual alkali carbonate liquid and the F-rich carbonate melt and 2) alkali ($Na_2O + K_2O$) enrichment of the coexisting nephelinite melt. The latter process likely contributed to the development of strong peralkalinity in the nephelinite melt.

Our study demonstrates the fundamental role of the alkali carbonate liquid phase in the formation of natrocarbonatites and strongly peralkaline nephelinites at Oldoinyo Lengai. We further suggest that in the geological past similar fluid-related process could also have resulted in strong peralkalinity in silicate melts occurring in rift tectonic settings worldwide.

Supplementary data to this article can be found online at https://doi.org/10.1016/j.gr.2020.03.013.

CRediT authorship contribution statement

Márta Berkesi: Conceptualization, Data curation, Formal analysis, Funding acquisition, Investigation, Methodology, Project administration, Resources, Validation, Visualization, Writing - original draft, Writing - review & editing. **Enikő Bali:** Data curation, Writing - original draft. **Robert J. Bodnar:** Writing - original draft. **Ábel Szabó:** Data curation, Writing - original draft. **Tibor Guzmics:** Conceptualization, Data curation, Formal analysis, Funding acquisition, Investigation, Methodology, Project administration, Resources, Validation, Visualization, Writing - original draft, Writing - review & editing.

Declaration of competing interest

The authors declare that they have no known competing financial interests or personal relationships that could have appeared to influence the work reported in this paper.

Acknowledgements

This study was financially supported by project NRDIO (National Research, Development, and Innovation Office of Hungary) K-119535 (to M. Berkesi and T. Guzmics) and by the Betta Üzletlánc Ltd. to Guzmics. In addition, M. Berkesi acknowledges to the ELTE Institutional Excellence Program (1783-3/2018/FEKUTSRAT) supported by the Hungarian Ministry of Human Capacities. We thank Toshiaki Tsunogae for his editorial handling, and Alan Cooper and an anonymous reviewer for their constructive comments that helped to improve the manuscript.

References

Bosshard-Stadlin, S.A., Mattson, H.B., Keller, J., 2014. Magma mixing and forced exsolution of CO_2 during the explosive 2007–2008 eruption of Oldoinyo Lengai (Tanzania). J. Volcanol. Geotherm. Res. 285, 229–246.

Brantley, S.L., Koepenick, K.W., 1995. Measured carbon dioxide emissions from Oldoinyo Lengai and the skewed distribution of passive volcanic fluxes. Geology 23, 933–936.

Church, A.A., Jones, A.P., 1995. Silicate-carbonate immiscibility at Oldoinyo Lengai. J. Petrol. 36, 869–889.

Cooper, A.F., Gittins, J., Tuttle, O.F., 1975. The system Na_2CO_3-K_2CO_3-$CaCO_3$ at 1 kilobar and its significance in carbonatite petrogenesis. Am. J. Sci. 275, 534–560.

Cooper, A.F., Palin, J.M., Collins, A.K., 2016. Fenitization of metabasic rocks by ferrocarbonatites at Haast River, New Zealand. Lithos 244, 109–121.

Dawson, J.B., 1962. The geology of Oldoinyo Lengai. Bull. Volcanol. 24, 349–387.

Dawson, J.B., 1998. Peralkaline nephelinite-natrocarbonatite relationships at Oldoinyo Lengai, Tanzania. J. Petrol. 39, 2077–2094.

Dawson, J.B., 2012. Nephelinite-melilite-carbonatite relationships: evidence from Pleistocene-recent volcanism in northern Tanzania. Lithos 152, 3–10.

Dawson, J.B., Smith, J.V., Steele, I.M., 1992. 1966 ash eruption of the of the carbonatite volcano Oldoinyo Lengai: mineralogy of lapilli and mixing of silicate and carbonate magmas. Mineral. Mag. 56, 1–16.

de Moor, J.M., Fischer, T.P., King, P.L., Botcharnikov, R.E., Hervig, R.L., Hilton, D.R., Barry, P.H., Mangasini, F., Ramirez, C., 2013. Volatile-rich silicate melts from Oldoinyo Lengai volcano (Tanzania): implications for carbonatite genesis and eruptive behavior. Earth Planet. Sci. Lett. 361, 379–390.

Donaldson, C.H., Dawson, J.B., Kanaris-Sotiriou, R., Batchelor, R.A., Walsh, J.N., 1987. The silicate lavas of Oldoinyo Lengai, Tanzania. J. Volcanol. Geotherm. Res. 37, 77–91.

Freestone, I.C., Hamilton, D.L., 1980. The role of liquid immiscibility in the genesis of carbonatites – and experimental study. Contrib. Mineral. Petr. 73, 105–117.

Frezzotti, M.L., Tecce, F., Casagli, A., 2012. Raman spectroscopy for fluid inclusion analysis. J. Geochem. Explor. 112, 1–20.

Gittins, J., Jago, B.C., 1998. Differentiation of natrocarbonatite magma at Oldoinyo Lengai volcano, Tanzania. Mineral. Mag. 62, 759–768.

Guzmics, T., Mitchell, R.H., Szabó, Cs., Berkesi, M., Milke, R., Ratter, K., 2012. Liquid immiscibility between silicate, carbonate and sulfide melts in melt inclusions hosted in co-precipitated minerals from kerimasi volcano (Tanzania): evolution of carbonated nephelinitic magma. Contrib. Mineral. Petr. 164, 101–122.

Guzmics, T., Berkesi, M., Bodnar, R.J., Fall, A., Bali, E., Milke, R., Vetlényi, E., Szabó, Cs., 2019. Natrocarbonatites: a hidden product of three-phase immiscibility. Geology 47, 527–530.

Hamilton, D.L., Freestone, I.C., Dawson, J.B., Donaldson, C.H., 1979. Origin of carbonatites by liquid immiscibility. Nature 279, 52–54.

Jago, B.C., Gittins, J., 1991. The role of fluorine in carbonatite magma evolution. Nature 349, 56–58.

Keller, J., Krafft, M., 1990. Effusive natrocarbonatite activity of Oldoinyo Lengai, June 1988. Bull. Volcanol. 52, 629–645.

Keller, J., Klaudius, J., Kervyn, M., Ernst, G.G.J., Mattsson, H.B., 2010. Fundamental changes in the activity of the natrocarbonatite volcano Oldoinyo Lengai, Tanzania I. New magma composition during the 2007–2008 explosive eruptions. Bull. Volcanol. 72, 893–912.

Kervyn, M., Ernst, G.G.J., Klaudius, J., Keller, J., Kervyn, F., Mattsson, H.B., Belton, F., Mbede, E., Jacobs, P., 2008. Voluminous lava flows at Oldoinyo Lengai in 2006: chronology of events and insights into the shallow magmatic system. Bull. Volcanol. 70, 1069–1086.

Kjarsgaard, B.A., Hamilton, D.L., Peterson, T.D., 1995. Peralkaline nephelinite/carbonatite liquid immiscibility: comparison of phase compositions in experiments and natural lavas from Oldoinyo Lengai. In: Bell, K., Keller, J. (Eds.), International Association of Volcanology and Chemistry of the Earth's Interior Proceedings in Volcanology 4: Carbonatite Volcanism—Oldoinyo Lengai and the Petrogenesis of Natrocarbonatite. Springer-Verlag, Berlin, pp. 163–190.

Klaudius, J., Keller, J., 2006. Peralkaline silicate lavas at Oldoinyo Lengai, Tanzania. Lithos 91, 173–190.

Koepenick, K.W., Brantley, S.L., Thompson, J.M., Rowe, G.L., Nyblade, A.A., Moshy, C., 1996. Volatile emissions from the crater and flank of Oldoinyo Lengai volcano, Tanzania. J. Geophys. Res. 101, 13819–13830.

Macdonald, R., Rogers, N.W., Fitton, J.G., Black, S., Smith, M., 2001. Plume-lithosphere interactions in the generation of the basalts of the Kenya Rift, East Africa. J. Petrol. 42, 877–900.

Mann, U., Marks, M., Markl, G., 2006. Influence of oxygen fugacity on mineral compositions in peralkaline melts: the Katzenbuckel volcano, Southwest Germany. Lithos 91, 262–285.

Marks, M.A.W., Markl, G., 2017. A global review on agpaitic rocks. Earth Sci. Rev. 173, 229–258.

Mattson, H.B., Reusser, E., 2010. Mineralogical and geochemical characterization of ashes from an early phase of the explosive September 2007 eruption of Oldoinyo Lengai (Tanzania). J. Afr. Earth Sci. 58, 752–763.

Mitchell, R.H., 2009. Peralkaline nephelinite–natrocarbonatite immiscibility and carbonatite assimilation at Oldoinyo Lengai, Tanzania. Contrib. Mineral. Petr. 158, 589–598.

Mitchell, R.H., Dawson, J.B., 2007. The 24th September 2007 ash eruption of the carbonatite volcano Oldoinyo Lengai, Tanzania: mineralogy of the ash and implications for formation of a newh ybrid magma type. Mineral. Mag. 71, 483–492.

Mitchell, R.H., Dawson, J.B., 2012. Carbonate–silicate immiscibility and extremely peralkaline silicate glasses from Nasira cone and recent eruptions at Oldoinyo Lengai Volcano, Tanzania. Lithos 152, 40–46.

Morse, S.A., 1980. Basalts and Phase Diagrams: An Introduction to the Quantitative Use of Phase Diagrams in Igneous Petrology. Springer New York (493 p.).

Nielsen, T.F.D., Veksler, I.V., 2002. Is natrocarbonatite a cognate fluid condensate? Contrib. Mineral. Petr. 142, 425–435.

Peterson, T.D., 1989. Peralkaline nephelinites. I. Comparative petrology of Shombole and Oldoinyo L'engai, East Africa. Contrib. Mineral. Petr. 101, 458–478.

Peterson, T.D., 1990. Petrology and genesis of natrocarbonatites. Contrib. Mineral. Petr. 105, 143–155.

Platz, T., Foley, S.F., André, L., 2004. Low-pressure fractionation of the Nyiragongo volcanic rocks, Virunga Province, D.R. Congo. J. Volcanol. Geotherm. Res. 136, 269–295.

Pyle, D.M., Pinkerton, H., Norton, G.E., Dawson, J.B., 1995. The dynamics of degassing at Oldoinyo Lengai. In: Bell, K., Keller, J. (Eds.), International Association of Volcanology and Chemistry of the Earth's Interior Proceedings in Volcanology 4: Carbonatite Volcanism—Oldoinyo Lengai and the Petrogenesis of Natrocarbonatite. Springer-Verlag, Berlin, pp. 37–46.

Rooney, T.O., 2019. The Cenozoic magmatism of East Africa: part V – magma sources and processes in the East African Rift. Lithos https://doi.org/10.1016/j.lithos.2019.105296 (in press).

Rossano, S., Mysen, B.O., 2012. Raman spectroscopy of silicate glasses and melts in geological systems. In: Dubessy, J., Cauon, M.-C., Rull, F. (Eds.), EMU Notes in Mineralogy. 12. Mineralogical Society of Great Britain & Ireland, pp. 319–364.

Sharygin, V.V., Kamenetsky, V.S., Zaitsev, A.N., Kamenetsky, M.B., 2012. Silicate–natrocarbonatite liquid immiscibility in 1917 eruption combeite–wollastonite nephelinite, Oldoinyo Lengai Volcano, Tanzania: melt inclusion study. Lithos 152, 23–39.

Thomas, R., Davidson, P., Schmidt, C., 2011. Extreme alkali bicarbonate- and carbonate-rich fluid inclusions in granite pegmatite from the Precambrian Rønne granite, Bornholm Island, Denmark. Contrib. Mineral. Petr. 161, 315–329.

Weidendorfer, D., Schmidt, M.W., Mattson, H.B., 2017. A common origin of carbonatite magmas. Geology 45, 507–510.

Weidendorfer, D., Schmidt, M.W., Mattson, H.B., 2019. Mineral resorption triggers explosive mixed silicate–carbonatite eruptions. Earth Planet. Sci. Lett. 510, 219–230.

Williams, Q., Knittle, E., 2003. Structural complexity in carbonatite liquid at high pressures. Geophys. Res. Lett. 30, 1022.

Woolley, A.R., Williams, C.T., Wall, F., Garcia, D., Moute, J., 1995. The Bingo carbonatite-ijolite-nepheline syenite complex, Zaire: geology, petrography, mineralogy and petrochemistry. J. Afr. Earth Sci. 21, 329–348.